The importance of ligand-induced backdonation in the stabilization of square planar d^{10} Nickel π-complexes

Addison N. Desnoyer,[†] Weiying He,[†] Shirin Behyan, Weiling Chiu, Jennifer A. Love,* and Pierre Kennepohl*[a]

Abstract: *The electronic nature of Ni π-complexes is underexplored even though they are widely postulated as intermediates in organometallic chemistry. Herein, we probe the geometric and electronic structure of a series of nickel π-complexes, Ni(dtbpe)(X) (dtbpe = 1,2-bis(di-tert-butyl)phosphinoethane; X = alkene or carbonyl containing π-ligands), using a combination of ^{31}P NMR, Ni K-edge XAS, Ni K_β XES, and DFT calculations. These complexes are best described as square planar d^{10} complexes with π-backbonding acting as the dominant contributor to M-L bonding to the π-ligand. The degree of backbonding correlates with $^2J_{PP}$ from NMR and the energy of the Ni 1s→4p$_z$ pre-edge in the Ni K-edge XAS data, and is determined by the energy of the π*$_{ip}$ ligand acceptor orbital. Thus, unactivated olefinic ligands tend to be poor π-acids whereas ketones, aldehydes, and esters allow for greater backbonding. However, backbonding is still significant even in cases where metal contributions are minor. In such cases, backbonding is dominated by charge donation from the diphosphine, which allows for strong backdonation even though the metal centre retains a formal d^{10} electronic configuration. This ligand-induced backbonding can be formally described as a 3-centre-4-electron (3c-4e) interaction where the nickel centre mediates charge transfer from the phosphine σ-donors to the π*$_{ip}$ ligand acceptor orbital. The implications of this bonding motif are described with respect to both geometric structure and reactivity.*

Introduction

Over the last two decades, renewed interest in the redox non-innocence of ligands has led to their proliferation in inorganic chemistry.[1,2] The use of these ligands as electron reservoirs enables two-electron processes from complexes which typically exhibit single-electron chemistry, particularly first-row transition metals.[3] In a pioneering example, Chirik and co-workers demonstrated that (PDI)Fe(N_2)$_2$ (PDI = 2,6-(2,6-^{i}Pr$_2$C$_6$H$_3$NCR)$_2$C$_5$H$_3$N, R = Me or Ph) catalyses the formal [2+2] cyclization of diolefins to form cyclobutane rings.[4] Notably, the iron centre stays in the Fe(II) oxidation state throughout the catalytic cycle, with the PDI ligand acting as a two-electron reservoir. More recently, the Tsurugi, Arnold, and Mashima groups reported that both the geometric and electronic non-innocence of α-diimine ligands plays a key role in niobium-catalysed chlorination of olefins, where the metal centre stays in the Nb(V) oxidation state and redox events occur on the diimine ligand.[5]

In contrast to these open-shell systems, closed-shell systems that rely on the ligand accepting and/or donating electron pairs are less common. A notable example of this type of reactivity is the zirconium system reported by Heyduk, which allows for a putative "oxidative addition" reaction to occur at a Zr(IV), d^0 metal centre.[6] In another example, we have recently shown that the oxidation of (TPA)Rh olefin complexes (TPA = tris(2-pyridylmethyl)amine) with H_2O_2 to form 2-rhodaoxetanes[7] is more accurately described as a ligand-centred oxidation,[8] rather than a metal-centred oxidation.[9] In this case, the π-ligand acts as a two-electron redox centre.

We have recently become interested in exploring the fundamental organometallic chemistry of earth-abundant, first-row transition metals. For example, we are exploring the organometallic chemistry of nickel,[10–14] which has undergone a renaissance in recent years.[15–21] Our focus has been the structure and reactivity of nickel π-complexes, which have been reported in a wide range of catalytic processes, including the coupling of CO_2 and ethylene,[5,22–32] intermolecular Tischenko coupling,[33–35] benzoxasilole synthesis,[36,37] the aldol reaction,[38] allylic alkylation,[39] allylic amination,[40] allylic amidation,[41] epoxide functionalization,[42] and Suzuki-Miyaura coupling.[43] Nickel π-complexes of heteroarenes have also been identified as key intermediates in nickel-catalysed catalyst transfer polycondensation to form polythiophenes.[44–56] Given the importance of nickel π-complexes, detailed exploration of their structure and reactivity is needed. Herein, we report the electronic structures of a series of nickel π-complexes relevant to catalysis. Additionally, we identify the impact of ancillary ligands in inducing and supporting π-backbonding, even in cases where metal contributions are limited.

In previous work, we noted that the ^{31}P{^{1}H} NMR spectroscopic data of a number of (dtbpe)Ni (dtbpe = 1,2-bis(di-*tert*-butyl)phosphino)ethane) π-complexes were consistent with typical d^{10} Ni(0) complexes (Chart 1).[10,11,57] In contrast, we also noted that the distorted square planar geometry with significant elongation of the π-bond were most consistent with a d^8 Ni(II) formulation, in keeping with the metallaepoxide extreme of the Dewar-Chatt-Duncanson (DCD) model of bonding (Scheme 1). In addition, preliminary density functional theory (DFT) calculations (*vide infra*) revealed *prohibitively* high barriers to rotation of the π-ligand (*i.e.* 80-100 kJ/mol), demonstrating that these complexes have a strong preference for the square planar geometry despite steric constraints. Experimentally, the ^{31}P{^{1}H} NMR spectrum of **1** up to 110 °C reveals no dynamical processes, indicating that the barrier to carbonyl inversion is *greater than* 70 kJ/mol. We have previously reported similar high barriers to rotation with a rhodium-olefin system.[8] Indeed, the metallaepoxide electromer of related nickel complexes have recently been invoked by the groups of Doyle[42] and Ogoshi[37] based on reactivity studies, and is also shown explicitly in Group 4 complexes that display similar structural parameters to the nickel species discussed here.[58–63] Ambiguity in the electronic structure of these nickel π-complexes hinders the effort towards rational design of nickel-catalysed processes. We thus set out to investigate the bonding and electronic structure of a family of (dtbpe)Ni complexes by utilizing a combination of spectroscopic and computational techniques.

[†] these authors contributed equally to this work
[a] Department of Chemistry, The University of British Columbia, 2036 Main Mall, Vancouver, BC, Canada V6T 1Z1
E-mail: jenlove@chem.ubc.ca, pierre@chem.ubc.ca

Chart 1 List of π-complexes considered in this study identified by their compound number (bold), τ_4 value, sums of the angles about the metal centre ($\sum \measuredangle_{Ni}$) and carbons in the π-ligand ($\sum \measuredangle_{C}$), C=X bond distance of the π-ligand (r_{CX}), and NMR P,P coupling constants (J_{PP})..

		τ_4	$\Sigma\measuredangle_{Ni}$	$\Sigma\measuredangle_{C}$	r_{CO} (pm)	$J_{P,P}$ (Hz)
1	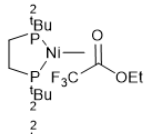	0.37	360.1°	341.7°	131.7	63
2	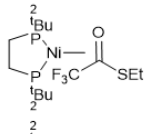	0.39	359.8°	345.4°	134.7	48
3	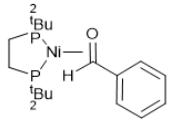	0.37	360.3°	351.7°	133.4	71
4	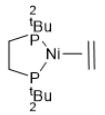	0.36	360.1°	352.6° 353.3°	141.9	-
5	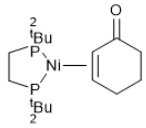	0.39	359.2°	352.3° 348.3°	141.6	61
6	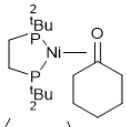	0.36	360.0°	344.7°	135.4	79
7	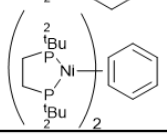	0.38	360.4°	355.4° 357.1°	142.1	-
	average	0.37	360.0°	350.3°	137.3	64

This study is also relevant to the ongoing discussion about the value of formal oxidation states.[64–66] Overall, we have found that these systems are dominated by π-backbonding with minimal σ-donation from the π-acidic ligand; the degree of backbonding reflects the π acidity of the ligand as well as the ability of the ancillary diphosphine ligands to induce π-backbonding mediated through the nickel 3*d* orbitals. We believe that this insight will prove beneficial to both the logical improvement of known catalytic reactions with nickel and to the rational design of new transformations.

Results and Discussion

Solid-state molecular structures

We selected a variety of (dtbpe)Ni complexes, ranging from well-defined nickel(II) complexes to π-complexes of organic molecules (Charts 1-3). The complexes were split into two categories based on the dihedral angles observed in the solid-state structures: (i) those with near planar geometries (**1-12**, where $\varphi_{dih} \sim 0°$ and $\sum \measuredangle_{Ni} \sim 360°$) and those with pseudo-tetrahedral geometries at the nickel centre (**13-15**, where $\varphi_{dih} \sim 90°$ and $\sum \measuredangle_{Ni} \sim 440°$). Alternatively, differences in the geometry of four-coordinate complexes can be evaluated using τ_4 values, which range from $\tau_4^{(D_{4h})} = 0$ to $\tau_4^{(T_d)} = 1$.[67] This approach confirms the *pseudo*-tetrahedral ($\sim T_d$) geometry of **13-15** (Chart 3), but suggests that the more planar complexes split into a set of highly symmetrical square planar complexes (Chart 2) and a set of complexes that deviate more strongly from idealized D_{4h} symmetry (Chart 1). The latter complexes are all π-complexes where the deviation from an idealized geometry results from the extremely small bite angle formed by the π-ligand (when considered as an η^2 ligand), even while maintaining planarity. The planar geometry at the metal centre implies that **1-7** exhibit a large degree of backbonding, which would typically be ascribed to the formation of square planar Ni(II) d^8 complexes (*i.e.*, a metallocyclic electronic configuration as depicted in Scheme 1).

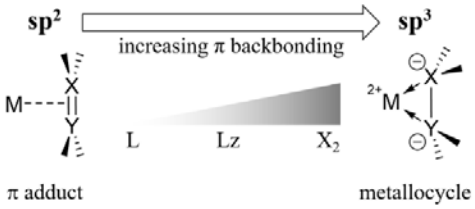

Scheme 1 Continuum of possible electronic configurations for binding of a π-system to a redox-active metal centre. On the left, is the limiting case of simple π-adduct formation, where M-L binding occurs via σ donation from the π-system. As π-backbonding increases, the X=Y π bond weakens and, in the limit, a metallacycle is formed with loss of the π bond and formal 2*e*⁻ oxidation at the metal centre.

The structure of the π-ligand itself has also frequently been used to estimate the degree of backbonding: electron donation into the ligand π* orbital *via* backbonding should lead to bond elongation. For example, Zeise's salt [$KPtCl_3(C_2H_4)$] and Cramer's dimer [$Rh(C_2H_4)_2Cl]_2$, both commonly used organometallic starting materials, feature short C=C ethylene bond distances of 137.5 pm[68] and 139.5 pm[69], respectively. In contrast, $(MeTPA)Rh(C_2H_4)(BPh_4)$, features a much longer C=C bond distance of 145 pm,[70] which corresponds to the metallacyclopropane end of the DCD spectrum. However, this method is generally qualitative, with many examples that fall in the middle of the spectrum being simply described as hybrids of the two resonance forms.[71,72] Indeed, the C=O bond lengths of the η^2-carbonyl complexes examined here (complexes **1**, **2**, **3** and **6**) all fall between 131.7-135.4 pm.[73–75] This range is unfortunately ambiguous, as it is in the middle of the typical bond lengths of ~122 pm and ~143 pm for C=O double bonds and C-O single bonds, respectively. Similarly, information about the degree of backbonding can be gleaned from the sum of the bond angles about the carbon atom of the π-unit ($\sum \measuredangle_C$, Chart 1). However, these results are again inconclusive, as the observed $\sum \measuredangle_C$ ($= 341 - 352°$) are intermediate between those expected for planar sp^2-hybridized and pyramidal sp^3-hybridized carbon atoms. This approach also suffers from the fact that many π-ligands bear hydrogen substituents, which can be difficult to locate using traditional X-ray diffraction (XRD)[76] and occasionally require neutron diffraction experiments to accurately ascertain their positions.

Chart 2. List of reference Ni(II) square planar complexes, which exhibit both small $^2J_{PP}$ coupling constants (where available) and τ_4 values.

		τ_4	$\Sigma\measuredangle_{Ni}$	$J_{P,P}$ (Hz)
8	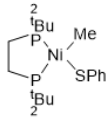	0.08	360.9°	4
9	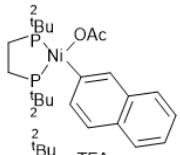	0.11	360.6°	-
10	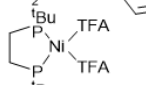	0.04	360.1°	-
11	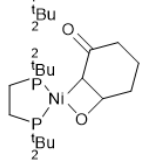	0.13	359.8°	6
12	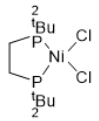	0.11	361.1°	-
	average	0.09	360.5°	5

Chart 3. List of reference pseudo-tetrahedral Ni(0) complexes, with large τ_4 values and $\sum\measuredangle_{Ni}$ > 400°.

		τ_4	$\Sigma\measuredangle_{Ni}$
13	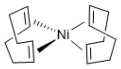	0.89	411.4°
14	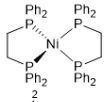	0.81	424.8°
15	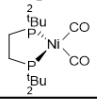	0.93	429.7°
	average	0.88	422.0°

Nuclear magnetic resonance spectroscopy

A common approach for evaluating the oxidation state of metals in diphosphine complexes involves using the magnitude of P,P-scalar coupling constants ($^2J_{P,P}$). In nickel chemistry, it is generally observed that small $^2J_{P,P}$ (i.e. 2-30 Hz) correspond to nickel(II) complexes whereas larger $^2J_{P,P}$ (i.e. 45-80 Hz) correspond to nickel(0) complexes.[10,11,22,77–84] However, exceptions to this trend have been reported by ourselves[10] and others.[84,85] Moreover, this approach is limited to asymmetric species as $^2J_{P,P}$ cannot be observed in complexes such as **4** and **7** due to symmetry.

Others have noted similar results with infrared (IR) spectroscopy of nickel carbonyl complexes[73] as we have found from XRD and NMR, i.e. that electron donation from the metal to the ligand does reduce the C=O bond, but to an extent that is ambiguously between a single and double bond. Importantly, none of these traditionally-used methods *directly* provides information about the electron density at the metal centre. We thus turned to X-ray absorption spectroscopy (XAS) and X-ray emission spectroscopy (XES) for an independent evaluation of the electronic structure and spectroscopic oxidation states at the metal. We sought to probe how a more direct measurement of Z_{eff} at the metal centre correlates to the above-discussed methods, in particular NMR spectroscopy. To the best of our knowledge, a study relating the magnitude of the NMR data (especially ^{31}P coupling constants) and how they correlate with alternate spectroscopic approaches has not been performed.

Ni K-edge X-ray absorption spectroscopy

In principle, the spectroscopic oxidation state of the metal ion can be accurately assigned *via* the energy of either the ionization edge and/or the low-energy pre-edge features in the metal K-edge near-edge spectrum.[86–92] Ni K-edge XAS can therefore be used to explore the spectroscopic oxidation state of a wide range of nickel-containing species.[93–97]

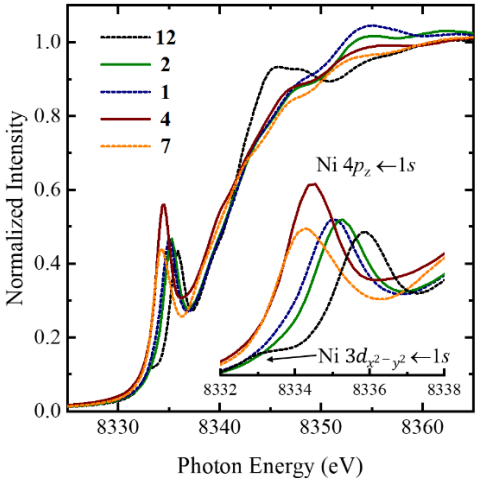

Figure 1. Normalized Ni K-edge PFY XANES edge spectra for Ni(dtbpe)Cl_2 (**12**), [Ni(dtbpe)]$_2$(benzene) (**7**), Ni(dtbpe)(ethylene) (**4**), Ni(dtbpe)CF_3COOEt (**1**), and Ni(dtbpe)CF_3COSEt (**2**). The pre-edge region for each of the spectra is shown in the inset with assignments for the observed features.

Ni K-edge XAS data was obtained for several Ni π-complexes, in addition to several reference complexes from Chart 1. Near-edge spectra for 'classic' Ni(II) complexes, such as that for complex **12,** have well-resolved pre-edge features: a weak feature at ~8333 eV and a more intense feature at ~8336 eV.

The weaker feature results from the electric-quadrupole allowed Ni 1s → 3d transition, whereas the more intense feature in such complexes has previously been ascribed to a dipole-allowed Ni 1s → 4p transition .[98,99] By contrast, Ni π-complexes (such as **1**, **2**, **4**, and **7**) have a markedly different edge profile and only one clearly resolvable intense pre-edge feature ranging from 8333-8336 eV. Similar spectroscopic behaviour has previously been observed in copper(I)-derived π-complexes.[87] As expected, the energy of the Ni 1s → 4p feature correlates with the oxidation state of the metal centre. The weaker pre-edge feature is not directly resolvable in most complexes, although in complexes **1** & **2** a weak low-energy shoulder is observed in the 2nd derivative of the spectra (see SI 04).

Ni K_β X-ray emission spectroscopy

To further explore the charge distribution, Ni K_β emission data was obtained for select complexes. The intensity-weighted average energy of the K_β line for each of the analysed complexes suggests a similar Z_{eff} (see SI 35). This trend is similar to that obtained from the energies of the Ni 1s → 4p feature in the Ni K-edge XAS. Indeed, the emission energies for the π-complexes **1-7** are quite similar (± 1 eV) and well separated from the observed energy of authentic Ni(II) complex **12**. The similarity in the K_β emission data for all of the π-complexes seems to support a common formal oxidation state for **1**-**7**.

Computational Studies - Density Functional Theory

DFT calculations were performed on each of the species in Chart 1 using simplified diphosphine ligands (See SI 01 for details). Molecular structures derived from B3LYP/def2-TZVP calculations of the dtbpe complexes, as well as those using a simplified diphosphine ligand (dmpe = 1,2-bis(dimethylphosphino) ethane),[A] yield good agreement with solid-state molecular structures of **1**-**12**.[10,11,22,57,100,101] The effect of decreasing the steric bulk and electron donation in the supporting diphosphine ligand does not affect the general structural trends and conclusions, which are consistent with those observed in the experimental data. Furthermore, the spectroscopic features observed in the Ni K-edge XAS data are well reproduced using TD-DFT analysis. Although qualitative results were consistent across a broad range of functionals, results from B3LYP provided the best agreement with experimental pre-edge features. Basis set effects were observed to be minimal beyond TZVP. The strong agreement with experimental data suggests that our DFT results should provide a reasonable description of bonding in these species.

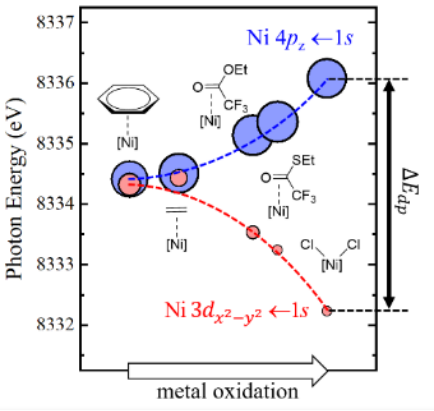

Figure 2. Calculated Ni K-edge XANES TD-DFT results for pre-edge region of the spectrum. Each complex is represented by a blue circle (Ni $4p_z$←1s) and a red circle (Ni $3d_{z2-y2}$←1s). The area of the of each circle is proportional to the calculated oscillator strength (f_{osc}) for each transition. All calculated TD-DFT energies at the Ni K-edge were shifted by -98.55 eV. [Ni] = Ni(dmpe).

The Ni K-edge pre-edge features are extremely sensitive to electron distribution (Figure 2). The more intense, higher energy ($Ni\ 4p_z \leftarrow 1s$) transition increases with greater oxidation at the metal centre and reproduces the trend observed in the experimental data. The weaker, low energy transition ($Ni\ 3d \leftarrow 1s$) shifts in the opposite direction, such that the energy difference between the two features (ΔE_{dp}) increases with increasing oxidation at the metal centre. The weak low-energy 3d feature should eventually be unresolvable from the higher intensity 4p feature, as observed in the experimental data.

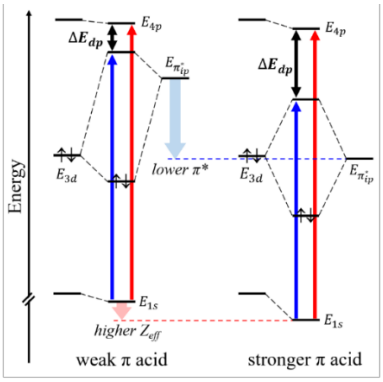

Figure 3. Simplified MO diagram depicting differences between weaker (left, *e.g.* ethylene in **4**) and stronger π-acidic ligands (right, e.g. cyclohexanone in **6**). Greater π-acidity leads to a much lower π^*_{ip} and thus greater π-backbonding. Decreased electron density at the metal centre (i.e. increased Z_{eff}) also lowers the energy of the Ni 1s orbital. These two effects lead to a simultaneous increase in energy of the Ni 1s → 4p transition (red arrow) and decrease in energy of the Ni 1s→ π* (blue arrow) and therefore an increase in the splitting of the two acceptor orbitals (ΔE_{dp}). Quantitative results are given in supporting information as SI 41.

The nature of the two pre-edge final states is consistent across the series of π-complexes. The intense feature results from a transition to the *non-bonding* Ni $4p_z$ orbital, whose energy directly reflects Z_{eff} at the metal centre. The weaker feature corresponds to a transition to the formally *ligand-based antibonding* π* orbital, which gains electric quadrupole character by mixing with the Ni $3d_{x2-y2}$ orbital through π-backbonding. In principle, the intensity of this features should therefore reflect the degree of M-L π-backbonding. However, the intensity of this pre-edge feature also depends on the degree of Ni d-p mixing, which varies across the series. This contribution, in addition to the difficulty of resolving weak pre-edge shoulder, makes it challenging to quantify the degree of backbonding from the experimental data.

To further explore the electron distribution in the ground state of these π-systems, we applied charge decomposition (CDA),[102,103] natural bond orbital (NBO),[104] and quantum theory of atoms-in-molecules (QTAIM)[105] analyses. Together, these provide a comprehensive view of the electronic properties of these systems. In all cases, the predominant interactions between the metal ion and the π-ligand can be well described using the basic interactions defined within the DCD bonding model.

Most notably, π-backbonding is the dominant contribution to bonding in these systems. The electron rich metal centre does not accept significant electron density through σ donation from the π_b ligand orbital with only minimal charge donation into the higher lying empty Ni 4s/p orbitals. The π-backbonding interaction involves overlap between the Ni $3d_{x2-y2}$ and the in-plane ligand π^* (π^*_{ip}). As expected, the overall degree of charge transfer correlates directly with the relative energies of these contributing fragment orbitals (see SI 41). Given that the Ni(dtbpe) fragment is

identical in all cases, differences within the series result primarily from changes in the energy of the ligand π^*_{ip} orbital. As summarized in Figure 3, poorer π-acids such as olefins have a higher energy $E_{\pi^*_{ip}}$ and thus should exhibit a small ΔE_{dp}, whereas $E_{\pi^*_{ip}}$ is lower in energy for stronger π-acids (such as carbonyls), increasing backbonding and a larger ΔE_{dp}.This interaction leads to a surprisingly large barrier for ligand rotation, even for those where backbonding is least important: barriers of ~100 kJ/mol are obtained for both symmetric (**4**) and asymmetric (**3**) π-ligands.

Table 1. Wiberg bond indices for Ni-C, Ni-X (X=O or most electron-rich C), and QTAIM $\nabla^2(\rho_{DFT})$ for optimized complexes at B3LYP/def2-TZVP level of theory.

		Wiberg Indices		$\nabla^2(\rho_{DFT})$		
		Ni-C	**Ni-X**	**bcp$_{NiC}$**	**bcp$_{NiX}$**	**rcp$_{NiCO}$**
	7'	0.362	0.357	0.217	0.224	0.309
C=C	**5'**	0.495	0.403	0.213	0.261	0.353
	4'	0.486	0.487	0.235	0.238	0.359
	3'	0.516	0.487	0.524	0.248	-
C=O	**1'**	0.556	0.468	0.550	0.219	-
	2'	0.552	0.502	0.537	0.243	-
	6'	0.523	0.494	0.536	0.232	-

Although the above analysis is valid for all species investigated, there is one additional factor that contributes to the nature of the bonding in these systems. The significant electronegativity difference between carbon and oxygen in the carbonyl π-ligands leads to asymmetry in the orbitals involved in bonding. Indeed, this bonding difference between olefins and carbonyls was identified by Eisenstein and Hoffmann nearly four decades ago.[73] The nature of bonding in these asymmetric systems is therefore more complex and deviates somewhat from the simple DCD model as σ donation becomes more localized from the terminal oxygen atom and π-backbonding localizes onto the electron deficient carbonyl carbon atom. This localization is also consistent with π-backbonding (to C) being stronger than σ-donation (from O), as observed from bond strength parameters in Table 1.

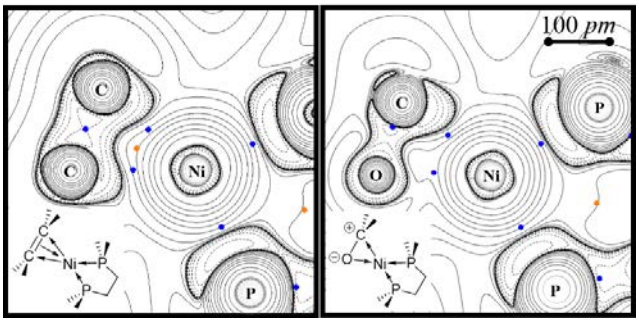

Figure 4. QTAIM topological analysis for complexes **4'** (left) and **1'** (right). Contour maps of $\nabla^2(\rho_{DFT})$ in the NiCX plane (X=C, O). Dotted contours refer to positive values of $\nabla^2(\rho_{DFT})$ and solid lines to negative values of $\nabla^2(\rho_{DFT})$. Bond critical points are shown in blue and ring critical points are shown in red. A simplified representation of these bonding interactions is shown on the bottom left of for each of the complexes.

The effect of π-ligand asymmetry is also clearly observed in the QTAIM analysis: Figure 4 shows a comparison of the Laplacian of the DFT-derived electron density ($\nabla^2(\rho_{DFT})$) for **4'** and **1'**. In the olefinic π-complex, the electron density within the Ni-C-C trigonal core reveals two Ni-C bond critical points (bcp) and one ring critical point (rcp) that connects all three atoms. The rcp correlates with a σ donor interaction due to π_{CC} donation in the Ni $3d_{xy}$ orbital and the two Ni-C bcp's correspond to π-backbonding from the Ni $3d_{x^2-y^2}$ and the ligand π^*_{ip}. By contrast, $\nabla^2(\rho_{DFT})$ for **1'** is highly asymmetric with two bcp's (Ni-O and Ni-C) but no discernible rcp in this case.

Discussion

Our studies of a series of nickel π-complexes reveal interesting electronic structure features that can be rationalized within the context of the DCD bonding model. The spectroscopic characteristics of these species are highly sensitive to the nature of bonding to the π-ligand, more specifically the properties of the species are intimately linked to the degree of π-backbonding from the electron-rich metal centre. Taken together, our studies allow for a more concrete evaluation of the factors that control this bonding and their implications.

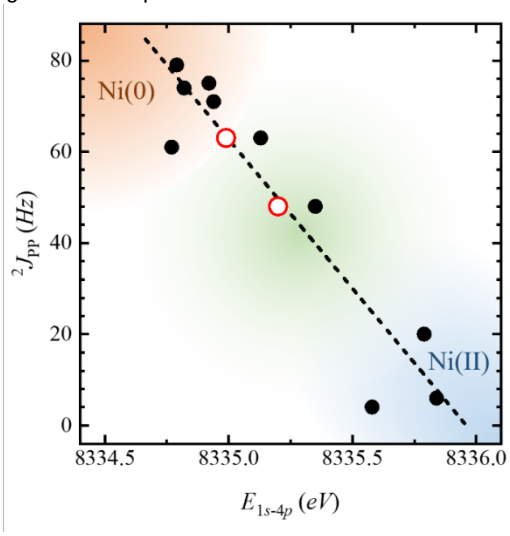

Figure 5. Correlation between Ni 1s→4p transition energies and $^2J_{PP}$ NMR coupling constants. Data points in black circles are from TDDFT calculations whereas those in red circles are from experimental Ni K-edge XAS data. All TD-DFT calculated transition energies were linearly shifted by -98.55 eV. The dashed line represents a linear correlation fit ($R^2 = 0.87$); see SI 3.

Oxidation states of nickel diphosphines are often evaluated *via* the magnitude of $^2J_{P,P}$ in unsymmetrical complexes: a small coupling constant ($2\ Hz < {}^2J_{P,P} < 30\ Hz$) correlates with Ni(II) complexes, whereas large coupling constants ($45\ Hz < {}^2J_{P,P} < 80\ Hz$) are associated with Ni(0) species. Differences reflect the electron density at the metal centre, which bridges the two ^{31}P atoms.[106] There is little evidence regarding potential Ni(I) species given the challenges associated with obtaining such information in paramagnetic species.[13,81] XAS offers the advantage of providing an independent experimental probe requiring neither inequivalent phosphorus ligands nor diamagnetism. As noted previously, the XAS data of formally square planar complexes

yield distinctive pre-edge features that track with oxidation of the metal centre. The NMR spectroscopy coupling constants and XAS pre-edge energies correlate extremely well (Figure 5), providing good support that $^2J_{P,P}$ (where available) are useful in defining electron density at the metal centre.

The fact that the two pre-edge features in the Ni K-edge XAS data respond so differently to changes in the electronic structure implies that they are sensitive to different aspects of the electronic structure of the metal centre. The Ni $4p_z$ orbital is out-of-plane from the most important ligand field interactions in pseudo square planar geometries and thus reports directly on Z_{eff} of the metal centre. In contrast, the weak pre-edge feature is a predominantly in-plane ligand-based final state with some metal $3d_{x^2-y^2}$ character. The two features therefore behave very differently with the former reporting on Z_{eff} of the metal centre and the latter on differences in the ligand field.

The DCD model is a simple yet powerful approach for explaining the behaviour of π-complexes in transition metal chemistry. Its limitations have recently been explored in copper dioxygen and related systems by invoking the important contributions of static correlation, specifically by allowing for multi-determinant solutions.[87] Since the electron density of these systems are well described from DFT calculations, we approached this same issue by applying natural resonance theory[107–109] (NRT) to expose different contributions to the overall electronic description (Table 2).[8] In all cases, the Ni(II) metallacycle contributes little to the overall electronic structure. The Ni(0) π-adduct and Ni(I) intermediate resonance structures account for >80% of the electronic structure in all cases. Indeed, we find that the Ni(0) π-adduct is the largest contributor for all the structures examined, although Ni(I) contributions are non-negligible.

Table 2. Summary of NRT analyses for complexes with either olefin or carbonyl π-ligands.

		Ni(0)	Ni(I)	Ni(II)
	7'	67%	33%	0%
C=C	5'	56%	37%	7%
	4'	51%	36%	10%
	3'	57%	38%	5%
C=O	1'	48%	47%	4%
	2'	46%	43%	11%

The high barrier to rotation for π-ligands in these complexes implies a surprisingly strong preference for a planar geometry even though a closed-shell Ni(0) π-adduct should not behave in this way. Even more surprisingly, the barrier to rotation does *not* correlate strongly with the degree of Ni(I) character from our NRT analysis. This effect points to the importance of the *trans*-diphosphine ligand in enabling and supporting π-backbonding. In principle, π-backbonding in a d^{10} Ni(0) occurs in any geometry of the π-ligand because of availability of filled Ni $3d_{xz,yz}$ orbitals that could also support backbonding. However, the C=C bond distance (r_{CC}) decreases significantly upon ligand rotation (from 147 to 139 pm), indicating that backbonding is not well supported in alternate geometries. The electronic changes that occur upon rotation of the π-ligand are an indicator of the importance of the diphosphine ligand.

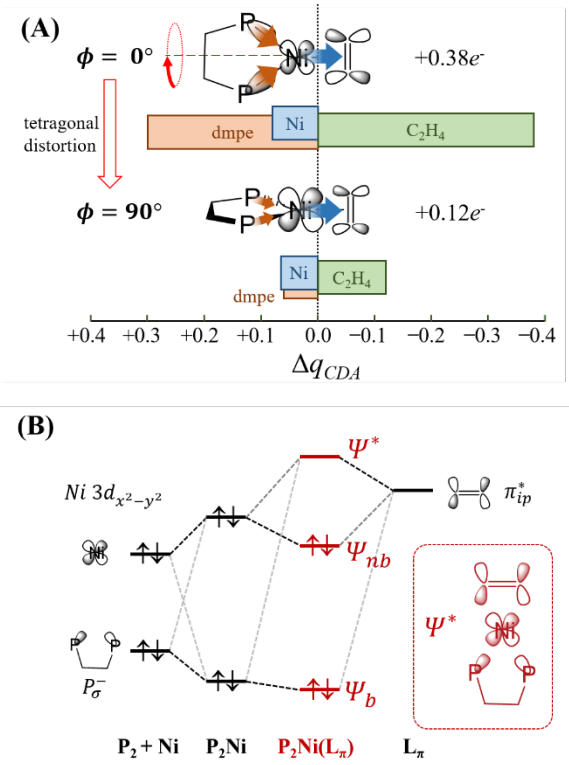

Figure 6. (**A**) DFT-calculated charge donation from CDA analysis for ethylene complex with dmpe ligand (**4'**) for ground state geometry ($\phi = 0°$) and after tetragonal distortion (rotation of NiCC plane relative to NiPP plane, $\phi = 90°$). Backbonding decreases substantially due to large drop in phosphine σ donation into the Ni $3d_{x2-y2}$. (**B**) Qualitative molecular orbital representation of the 3c4e bonding that connects P_σ^- with π_{ip}^* via the Ni $3d_{x^2-y^2}$ orbital.

Charge donation from the P_2Ni fragment to the π-ligand decreases substantially when the diphosphine ligand is perpendicular to the Ni $3d_{x^2-y^2}$ donor orbital (Figure 6A). This suggests that the metal centre in these complexes mediates charge donation from the electron rich diphosphine to the ethylene π*. The orbital contributions that allow for π-backbonding are reminiscent of a classical 3c-4e bond; in this situation the three contributing orbitals are the antisymmetric combination of the phosphine σ-donor orbitals (P_σ^-, 2 valence electrons), the Ni $3d_{x^2-y^2}$ (2 valence electrons), and the ligand π_{ip}^* orbital (Figure 6B). In this geometry, the two sets of ligands generate a cooperative "push-pull" system mediated by the metal centre in a manner similar to that which has been observed in cytochrome P450s.[110] This $\sigma \rightarrow \pi$ cooperative interaction mediation by the metal centre is only possible in specific geometries and is essentially identical to mixed σ/π interactions observed in trigonal systems.(ref – π contributions in tbp complexes). This would preclude similar effects with ancillary ligands that enforce a linear geometry in Ni(0) complexes, such as N-heterocyclic carbenes (NHCs). It is noteworthy that Itami[111] and Liu[112] have identified striking reactivity differences in the catalytic activity of monodentate phosphines versus their bidentate analogues, with additional computational studies performed by Houk.[112]

Although all of the olefin complexes investigated are best described as Ni(0) complexes, highly electron poor carbonyl complexes have significantly more oxidized metal centres. Complexes **1** and **2** represent intriguing examples of intermediate cases that are shifting towards a "Ni(I)"-type description. The CF_3 substituent at the carbonyl carbon increases their π-acidity substantially. However, the ester ligand in **1** is less π-acidic than the equivalent thioester in **2** due to better delocalization of the ligand π-system, which simultaneously decreases overlap of the π* with the Ni $3d_{x2-y2}$ and increases its energy. In **2**, poor π-overlap between the larger atomic orbitals on sulphur and the carbonyl π* allows for significant backbonding in this case. These differences should lead to concomitant differences in reactivity.

Indeed, **1** and **2** display fundamentally different reactivity. In refluxing benzene, **2** slowly thermolyses over two days, resulting in complex **15**, free ligand, and thioester, as determined by $^{31}P\{^1H\}$ and ^1H NMR spectroscopy. In contrast, complex **1** is stable for up to a week under the same conditions with no sign of decomposition. Complex **1** does not react with MeLi, even upon prolonged reflux in benzene, but under the same conditions, complex **2** reacts with MeLi to form trace amounts of EtSSEt. In addition, complex **2** is susceptible to cross-coupling with phenylboronic acid, forming PhSEt in moderate (35%) yield.[11] No such cross-coupling reactivity was observed with complex **1**. Lastly, complexes **1** and **2** react differently with MeI. Upon refluxing in benzene for 12 hours, **1** forms (dtbpe)Ni(Me)(I),[113] which was verified by ^{31}P NMR spectroscopy, and liberates the free ester, whereas complex **2** does not react with MeI at all under the same conditions.[B] Such behaviour is consistent with reduced π-donation of the ester in **1**, allowing for its displacement by MeI.

Conclusions

Our spectroscopic and computational studies on a series of Ni π-complexes shed light on an intriguing effect whereby σ-donor ancillary ligands are instrumental in stabilizing a square-planar geometry in formally d^{10} nickel(0) complexes. In the case of olefinic complexes, the evidence shows that these are best described as Ni(0) π-adducts with strong π-backbonding coupled to in-plane σ donation from the supporting electron rich diphosphine bidentate ligand. The formation of this 3c-4e interaction generates ligand σ-to-π (Lσ→Lπ) charge transfer. This ligand-induced (push-pull) π-backbonding is responsible for the large observed rotational barrier about the π-ligand even with relatively poor π-acidic ligands such as ethylene. This unique electronic structure can play an important role in the reactivity of such species.[114] The situation is more complex in situations with highly electron poor π-systems, where metal-centred backbonding increases and leads to Ni(I) character becomes significantly more important. The implication here for catalyst design is that the orbital energies of the unsaturated substrate can be matched not only with the metal centre but with the diphosphine ligand. We anticipate that the tuning of both electron-donating diphosphine and the electron-accepting π-ligand will allow for an additional handle in the design of subsequent catalysts, and that more detailed studies of ancillary ligand effects in such systems are warranted.

Experimental Section

General Considerations

Unless stated otherwise, all reactions were performed in a glovebox or on a Schlenk line under an atmosphere of pure N_2 using standard Schlenk techniques. Anhydrous pentanes, toluene, diethyl ether, and tetrahydrofuran were purchased from Aldrich, sparged with N_2, and dried further by passage through towers containing activated alumina and molecular sieves. C_6H_6 and C_6D_6 were purchased from Aldrich and dried over sodium/benzophenone before being distilled and degassed by three freeze-pump-thaw cycles. CD_2Cl_2 was purchased from Aldrich and dried over CaH_2 before being distilled and degassed by three freeze-pump-thaw cycles. $Ni(COD)_2$ (**13**) was purchased from Strem and used as received. Compounds **1-2**,[11] **3**,[57] **4**,[100] **5-6**,[10] **7**,[115] **8-10**,[11] **11**,[10] **12**,[113] **14**,[116] and **15**[100] were prepared according to literature procedures. All other chemicals were purchased from commercial suppliers and used as received.

X-ray Absorption Spectroscopy

All the XAS samples were analysed as solids under anaerobic conditions and diluted in boron nitride (20-50% by weight). XAS Ni K-edges were acquired at the SSRL beamline 7-3, which is equipped with a Si(220) ϕ = 90° double crystal monochromator, a 9 keV cutoff mirror, and a He cryostat (at 20 K). Data were collected using a Canberra 30-element Ge solid-state detector with a 3mm Co filter. Data averaging and energy calibration were performed using SixPack[117] and the AUTOBK algorithm available in the Athena software package[118] was employed for data reduction and normalization. Independent fitting was also performed using BlueprintXAS.[119,120]

X-ray emission spectroscopy

Samples were prepared for XES by pressing finely ground powders into 1 mm Al spacers, and sealing with 40 μm Kapton tape. Data were obtained at the Cornell High Energy Synchrotron Radiation Source (CHESS) at the C-line end station. Energy selection was performed with upstream multilayers, providing ~50 eV band pass. A Rh-coated harmonic rejection mirror was also utilized. K_β X-ray emission spectra were measured using a spherical analyzer (using the 620 reflection of three Ge 310 analyzer crystals) in combination with a silicon drift detector aligned in Rowland geometry. Data were normalized with respect to the incident flux in an upstream N_2-filled ionization chamber. Data were collected at ~20 K in a Displex cryostat to minimize photoreduction.

Computational methods

Initial geometries for all molecules were obtained from crystallographic coordinates (where available) or constructed from standard models. Geometry optimizations and numerical frequency calculations were performed using version 3.0.3 of the ORCA computational chemistry package. Molecular geometries were optimized using the B3LYP functional in combination with the Ahlrichs triple-ζ basis set with valence polarization (def2-TZVP) for all atoms. Computational efficiency was improved by applying the RI approximation (RIJCOSX) for the hybrid functional. All calculations were performed with integration grid 4. Reported thermochemical energies are given in kJ/mol and correspond to Gibbs free energies (ΔG^0) with zero-point vibrational energy corrections (ZPVE). NBO results were obtained using Gaussian 09; AIM and CDA calculation were performed in Multiwfn software from NBO outputs. All calculations were run on either the Abacus (UBC Chemistry) or GREX (Westgrid) computing clusters.

Acknowledgements

This work was supported by the Natural Sciences and Engineering Research Council of Canada (NSERC) via Discovery grants and Research Tools and Instrumentation grants to J.A.L. and P.K. Scholarship support was provided to A.N.D. by NSERC (CGS-D3 + MSFSS), the University of British Columbia (Laird + 4YF), and the Izaak Walton Killam Foundation during his graduate studies. W.H. is grateful for support in the form of a MITACS Globalink doctoral fellowship. W.C. is grateful for support from the NSERC CREATE SusSyn program.

This work is partially based upon research performed at the Stanford Synchrotron Radiation Lightsource (SSRL) at the SLAC National Accelerator Laboratory. Use of SSRL is supported by the U.S. Department of Energy, Office of Science, Office of Basic Energy Sciences under Contract No. DE-AC02-76SF00515. This work is partially based upon research conducted at the Cornell High Energy Synchrotron Source (CHESS) which is supported by the National Science Foundation under award DMR-1332208. This research was enabled in part by support provided by WestGrid (www.westgrid.ca) and Compute Canada Calcul Canada (www.computecanada.ca).

[A] Computed structures using the dmpe ligand are labeled using a ‘ (prime) in the numbering. For example, **4’** is simply complex **4** from Chart 1 that has been calculated using the simplified dmpe ligand rather than the full dtbpe ligand.

[B] Both **1** and **2** react with HCl to make (dtbpe)$NiCl_2$ (**12**) and PhLi to form moderate but irreproducible amounts of biphenyl.

[1] O. R. Luca, R. H. Crabtree, *Chem. Soc. Rev.* **2013**, *42*, 1440–1459.

[2] V. Lyaskovskyy, B. de Bruin, *ACS Catal.* **2012**, *2*, 270–279.

[3] P. J. Chirik, K. Wieghardt, *Science* **2010**, *327*, 794–795.

[4] M. W. Bouwkamp, A. C. Bowman, E. Lobkovsky, P. J. Chirik, *J. Am. Chem. Soc.* **2006**, *128*, 13340–13341.

[5] H. Nishiyama, H. Ikeda, T. Saito, B. Kriegel, H. Tsurugi, J. Arnold, K. Mashima, *J. Am. Chem. Soc.* **2017**, *139*, 6494–6505.

[6] K. J. Blackmore, J. W. Ziller, A. F. Heyduk, *Inorg. Chem.* **2005**, *44*, 5559–5561.

[7] B. de Bruin, M. J. Boerakker, J. J. J. M. Donners, B. E. C. Christiaans, P. P. J. Schlebos, R. de Gelder, J. M. M. Smits, A. L. Spek, A. W. Gal, *Angew. Chem.* **1997**, *36*, 2064–2067.

[8] A. N. Desnoyer, S. Behyan, B. O. Patrick, A. Dauth, J. A. Love, P. Kennepohl, *Inorg. Chem.* **2016**, *55*, 13–15.

[9] P. H. M. Budzelaar, A. N. J. Blok, *Eur. J. Inorg. Chem.* **2004**, *2004*, 2385–2391.

[10] A. N. Desnoyer, E. G. Bowes, B. O. Patrick, J. A. Love, *J. Am. Chem. Soc.* **2015**, *137*, 12748–12751.

[11] A. N. Desnoyer, F. W. Friese, W. Chiu, M. W. Drover, B. O. Patrick, J. A. Love, *Chem. Eur. J.* **2016**, *22*, 4070–4077.

[12] N. A. LaBerge, J. A. Love, *Eur. J. Org. Chem.* **2015**, *2015*, 5546–5553.

[13] D. D. Beattie, E. G. Bowes, M. W. Drover, J. A. Love, L. L. Schafer, *Angew. Chem.* **2016**, *55*, 13290–13295.

[14] A. N. Desnoyer, J. Geng, M. W. Drover, B. O. Patrick, J. A. Love, *Chem. Eur. J.* **2017**, *23*, 11509–11512.

[15] D. R. Hartline, M. Zeller, C. Uyeda, *J. Am. Chem. Soc.* **2017**, *139*, 13672–13675.

[16] D. J. Mindiola, *Angew. Chem.* **2009**, *48*, 6198–6200.

[17] P. Zimmermann, C. Limberg, *J. Am. Chem. Soc.* **2017**, *139*, 4233–4242.

[18] E. B. Corcoran, M. T. Pirnot, S. Lin, S. D. Dreher, D. A. DiRocco, I. W. Davies, S. L. Buchwald, D. W. C. MacMillan, *Science* **2016**, *353*, 279–283.

[19] B. A. Vara, X. Li, S. Berritt, C. R. Walters, E. J. Petersson, G. A. Molander, *Chem. Sci.* **2018**, *9*, 336–344.

[20] B. P. Woods, M. Orlandi, C.-Y. Huang, M. S. Sigman, A. G. Doyle, *J. Am. Chem. Soc.* **2017**, *139*, 5688–5691.

[21] C. Heinz, J. P. Lutz, E. M. Simmons, M. M. Miller, W. R. Ewing, A. G. Doyle, *J. Am. Chem. Soc.* **2018**, *140*, 2292–2300.

[22] M. L. Lejkowski, R. Lindner, T. Kageyama, G. É. Bódizs, P. N. Plessow, I. B. Müller, A. Schäfer, F. Rominger, P. Hofmann, C. Futter, et al., *Chem. Eur. J.* **2012**, *18*, 14017–14025.

[23] N. Saito, Z. Sun, Y. Sato, *Chem. Asian J.* **2015**, *10*, 1170–1176.

[24] S. C. E. Stieber, N. Huguet, T. Kageyama, I. Jevtovikj, P. Ariyananda, A. Gordillo, S. A. Schunk, F. Rominger, P. Hofmann, M. Limbach, *Chem. Commun.* **2015**, *51*, 10907–10909.

[25] M. Al-Ghamdi, S. V. C. Vummaleti, L. Falivene, F. A. Pasha, D. J. Beetstra, L. Cavallo, *Organometallics* **2017**, *36*, 1107–1112.

[26] Z. R. Greenburg, D. Jin, P. G. Williard, W. H. Bernskoetter, *Dalton Trans.* **2014**, *43*, 15990–15996.

[27] I. Knopf, D. Tofan, D. Beetstra, A. Al-Nezari, K. Al-Bahily, C. C. Cummins, *Chem. Sci.* **2017**, *8*, 1463–1468.

[28] C. Hendriksen, E. A. Pidko, G. Yang, B. Schäffner, D. Vogt, *Chem. Eur. J.* **2014**, *20*, 12037–12040.

[29] N. Huguet, I. Jevtovikj, A. Gordillo, M. L. Lejkowski, R. Lindner, M. Bru, A. Y. Khalimon, F. Rominger, S. A. Schunk, P. Hofmann, et al., *Chem. Eur. J.* **2014**, *20*, 16858–16862.

[30] D. Jin, P. G. Williard, N. Hazari, W. H. Bernskoetter, *Chem. Eur. J.* **2014**, *20*, 3205–3211.

[31] S. Manzini, N. Huguet, O. Trapp, T. Schaub, *Eur. J. Org. Chem.* **2015**, *2015*, 7122–7130.

[32] W. Guo, C. Michel, R. Schwiedernoch, R. Wischert, X. Xu, P. Sautet, *Organometallics* **2014**, *33*, 6369–6380.

[33] S. Ogoshi, Y. Hoshimoto, M. Ohashi, *Chem. Commun.* **2010**, *46*, 3354.

[34] Y. Hoshimoto, M. Ohashi, S. Ogoshi, *J. Am. Chem. Soc.* **2011**, *133*, 4668–4671.

[35] Y. Hoshimoto, M. Ohashi, S. Ogoshi, *Acc. Chem. Res.* **2015**, *48*, 1746–1755.

[36] R. Kumar, Y. Hoshimoto, H. Yabuki, M. Ohashi, S. Ogoshi, *J. Am. Chem. Soc.* **2015**, *137*, 11838–11845.

[37] Y. Hoshimoto, H. Yabuki, R. Kumar, H. Suzuki, M. Ohashi, S. Ogoshi, *J. Am. Chem. Soc.* **2014**, *136*, 16752–16755.

[38] Y. Bernhard, B. Thomson, V. Ferey, M. Sauthier, *Angew. Chem.* **2017**, *56*, 7460–7464.

[39] Y. Kita, R. D. Kavthe, H. Oda, K. Mashima, *Angew. Chem.* **2016**, *55*, 1098–1101.

[40] Y. Kita, H. Sakaguchi, Y. Hoshimoto, D. Nakauchi, Y. Nakahara, J.-F. Carpentier, S. Ogoshi, K. Mashima, *Chem. Eur. J.* **2015**, *21*, 14571–14578.

[41] M. S. Azizi, Y. Edder, A. Karim, M. Sauthier, *Eur. J. Org. Chem.* **2016**, *2016*, 3796–3803.

[42] D. K. Nielsen, A. G. Doyle, *Angew. Chem.* **2011**, *50*, 6056–6059.

[43] K. Muto, J. Yamaguchi, D. G. Musaev, K. Itami, *Nat. Commun.* **2015**, *6*, 7508.

[44] M. L. Smith, A. K. Leone, P. M. Zimmerman, A. J. McNeil, *ACS Macro Lett.* **2016**, *5*, 1411–1415.

[45] A. K. Leone, A. J. McNeil, *Acc. Chem. Res.* **2016**, *49*, 2822–2831.

[46] B. C. Achord, J. W. Rawlins, *Macromolecules* **2009**, *42*, 8634–8639.

[47] R. Miyakoshi, A. Yokoyama, T. Yokozawa, *J. Am. Chem. Soc.* **2005**, *127*, 17542–17547.

[48] M. C. Iovu, E. E. Sheina, R. R. Gil, R. D. McCullough, *Macromolecules* **2005**, *38*, 8649–8656.

[49] P. Willot, G. Koeckelberghs, *Macromolecules* **2014**, *47*, 8548–8555.

[50] S. R. Lee, J. W. G. Bloom, S. E. Wheeler, A. J. McNeil, *Dalton Trans.* **2013**, *42*, 4218.

[51] Z. J. Bryan, A. J. McNeil, *Chem. Sci.* **2013**, *4*, 1620.

[52] S. R. Lee, Z. J. Bryan, A. M. Wagner, A. J. McNeil, *Chem. Sci.* **2012**, *3*, 1562.

[53] E. L. Lanni, J. R. Locke, C. M. Gleave, A. J. McNeil, *Macromolecules* **2011**, *44*, 5136–5145.
[54] H. Komber, V. Senkovskyy, R. Tkachov, K. Johnson, A. Kiriy, W. T. S. Huck, M. Sommer, *Macromolecules* **2011**, *44*, 9164–9172.
[55] R. Tkachov, V. Senkovskyy, H. Komber, J.-U. Sommer, A. Kiriy, *J. Am. Chem. Soc.* **2010**, *132*, 7803–7810.
[56] E. L. Lanni, A. J. McNeil, *J. Am. Chem. Soc.* **2009**, *131*, 16573–16579.
[57] A. N. Desnoyer, W. Chiu, C. Cheung, B. O. Patrick, J. A. Love, *Chem. Commun.* **2017**, *53*, 12442–12445.
[58] G. Erker, U. Dorf, P. Czisch, J. L. Peterson, *Organometallics* **1986**, *5*, 668–676.
[59] G. Erker, U. Dorf, J. L. Atwood, W. E. Hunter, *J. Am. Chem. Soc.* **1986**, *108*, 2251–2257.
[60] F. R. Askham, K. M. Carroll, S. J. Alexander, A. L. Rheingold, B. S. Haggerty, *Organometallics* **1993**, *12*, 4810–4815.
[61] J. E. Hill, P. E. Fanwick, I. P. Rothwell, *Organometallics* **1992**, *11*, 1771–1773.
[62] G. Fachinetti, C. Biran, C. Floriani, A. Chiesi-Villa, C. Guastini, *J. Am. Chem. Soc.* **1978**, *100*, 1921–1922.
[63] L. Li, K. E. Kristian, A. Han, J. R. Norton, W. Sattler, *Organometallics* **2012**, *31*, 8218–8224.
[64] P. T. Wolczanski, *Organometallics* **2017**, *36*, 622–631.
[65] G. Parkin, *J. Chem. Educ.* **2006**, *83*, 791.
[66] M. L. H. Green, G. Parkin, *J. Chem. Educ.* **2014**, *91*, 807–816.
[67] L. Yang, D. R. Powell, R. P. Houser, *Dalton Trans.* **2007**, 955–964.
[68] M. Benedetti, C. R. Barone, D. Antonucci, V. M. Vecchio, A. Ienco, L. Maresca, G. Natile, F. P. Fanizzi, *Dalton Trans.* **2012**, *41*, 3014.
[69] "Wadepohl CCDC private communication," **n.d.**
[70] B. de Bruin, M. J. Boerakker, J. A. W. Verhagen, R. de Gelder, J. M. M. Smits, A. W. Gal, *Chem. Eur. J.* **2000**, *6*, 298–312.
[71] L. E. Doyle, W. E. Piers, J. Borau-Garcia, M. J. Sgro, D. M. Spasyuk, *Chem. Sci.* **2016**, *7*, 921–931.
[72] L. E. Doyle, W. E. Piers, J. Borau-Garcia, *J. Am. Chem. Soc.* **2015**, *137*, 2187–2190.
[73] J. Kaiser, J. Sieler, D. Walther, E. Dinjus, L. Golic, *Acta Crystallogr. Sect. B Struct. Crystallogr. Cryst. Chem.* **1982**, *38*, 1584–1586.
[74] T. T. Tsou, J. C. Huffman, J. K. Kochi, *Inorg. Chem.* **1979**, *18*, 2311–2317.
[75] R. Countryman, B. R. Penfold, *J. Chem. Soc. D Chem. Commun.* **1971**, 1598.
[76] M. Bühl, M. Håkansson, A. H. Mahmoudkhani, L. Öhrström, *Organometallics* **2000**, *19*, 5589–5596.
[77] P. N. Plessow, L. Weigel, R. Lindner, A. Schäfer, F. Rominger, M. Limbach, P. Hofmann, *Organometallics* **2013**, *32*, 3327–3338.
[78] J. J. Garcia, W. D. Jones, *Organometallics* **2000**, *19*, 5544–5545.
[79] J. J. Garcia, N. M. Brunkan, W. D. Jones, *J. Am. Chem. Soc.* **2002**, *124*, 9547–9555.
[80] T. A. Ateşin, T. Li, S. Lachaize, W. W. Brennessel, J. J. García, W. D. Jones, *J. Am. Chem. Soc.* **2007**, *129*, 7562–7569.
[81] D. J. Mindiola, R. Waterman, D. M. Jenkins, G. L. Hillhouse, *Inorg. Chim. Acta* **2003**, *345*, 299–308.
[82] R. Waterman, G. L. Hillhouse, *J. Am. Chem. Soc.* **2008**, *130*, 12628–12629.
[83] J. J. Curley, K. D. Kitiachvili, R. Waterman, G. L. Hillhouse, *Organometallics* **2009**, *28*, 2568–2571.
[84] D. J. Mindiola, R. Waterman, V. M. Iluc, T. R. Cundari, G. L. Hillhouse, *Inorg. Chem.* **2014**, *53*, 13227–13238.
[85] R. Doi, K. Kikushima, M. Ohashi, S. Ogoshi, *J. Am. Chem. Soc.* **2015**, *137*, 3276–3282.
[86] J. E. Penner-Hahn, in *Compr. Coord. Chem. II From Biol. to Nanotechnol.* (Eds.: A.B.P. Lever, J.A. McCleverty, T.J. Meyer), Elsevier Pergamon, **2005**, pp. 159–186.
[87] N. C. Tomson, K. D. Williams, X. Dai, S. Sproules, S. DeBeer, T. H. Warren, K. Wieghardt, *Chem. Sci.* **2015**, *6*, 2474–2487.
[88] T. E. Westre, P. Kennepohl, J. G. DeWitt, B. Hedman, K. O. Hodgson, E. I. Solomon, *J. Am. Chem. Soc.* **1997**, *119*, 6297–6314.
[89] S. N. MacMillan, K. M. Lancaster, *ACS Catal.* **2017**, *7*, 1776–1791.
[90] J. L. DuBois, P. Mukherjee, T. D. P. Stack, B. Hedman, E. I. Solomon, K. O. Hodgson, *J. Am. Chem. Soc.* **2000**, *122*, 5775–5787.
[91] J. Kowalska, S. DeBeer, *Biochim. Biophys. Acta - Mol. Cell Res.* **2015**, *1853*, 1406–1415.
[92] T. Yamamoto, *X-Ray Spectrom.* **2008**, *37*, 572–584.
[93] A. Kuzmin, N. Mironova, J. Purans, A. Rodionov, *J. Phys. Condens. Matter* **1995**, *7*, 9357–9368.
[94] A. Corrias, G. Mountjoy, G. Piccaluga, S. Solinas, *J. Phys. Chem. B* **1999**, *103*, 10081–10086.
[95] A. Rougier, C. Delmas, A. V. Chadwick, *Solid State Commun.* **1995**, *94*, 123–127.
[96] I. J. Pickering, G. N. George, J. T. Lewandowski, A. J. Jacobson, *J. Am. Chem. Soc.* **1993**, *115*, 4137–4144.
[97] A. N. Mansour, C. A. Melendres, *J. Phys. Chem. A* **1998**, *102*, 65–81.
[98] C. Gougoussis, M. Calandra, A. Seitsonen, C. Brouder, A. Shukla, F. Mauri, *Phys. Rev. B - Condens. Matter Mater. Phys.* **2009**, *79*, 045118.
[99] J. Cho, R. Sarangi, J. Annaraj, S. Y. Kim, M. Kubo, T. Ogura, E. I. Solomon, W. Nam, *Nat. Chem.* **2009**, *1*, 568–572.
[100] K.-R. Pörschke, C. Pluta, B. Proft, F. Lutz, C. Krüger, *Zeitschrift für Naturforsch. B* **1993**, *48*, 608–626.
[101] M. Schultz, P.-N. Plessow, F. Rominger, L. Weigel, *Acta Crystallogr. Sect. C Cryst. Struct. Commun.* **2013**, *69*, 1437–1447.
[102] M. Joost, L. Estévez, S. Mallet-Ladeira, K. Miqueu, A. Amgoune, D. Bourissou, *Angew. Chem.* **2014**, *53*, 14512–14516.
[103] S. Dapprich, G. Frenking, *J. Phys. Chem.* **1995**, *99*, 9352–9362.
[104] A. E. Reed, L. a Curtiss, F. Weinhold, *Chem. Rev.* **1988**, *88*, 899–926.
[105] L. J. Farrugia, C. Evans, D. Lentz, M. Roemer, *J. Am. Chem. Soc.* **2009**, *131*, 1251–1268.
[106] R. D. Bertrand, F. B. Ogilvie, J. G. Verkade, *J. Am. Chem. Soc.* **1970**, *92*, 1908–1915.
[107] E. D. Glendening, F. Weinhold, *J. Comput. Chem.* **1998**, *19*, 593–609.
[108] E. D. Glendening, F. Weinhold, *J. Comput. Chem.* **1998**, *19*, 610–627.
[109] E. D. Glendening, J. K. Badenhoop, F. Weinhold, *J. Comput. Chem.* **1998**, *19*, 628–646.
[110] J. T. Groves, *Nat. Chem.* **2014**, *6*, 89–91.
[111] K. Muto, J. Yamaguchi, K. Itami, *J. Am. Chem. Soc.* **2012**, *134*, 169–172.
[112] Z. Li, S.-L. Zhang, Y. Fu, Q.-X. Guo, L. Liu, *J. Am. Chem. Soc.* **2009**, *131*, 8815–8823.
[113] I. Bach, R. Goddard, C. Kopiske, K. Seevogel, K.-R. Pörschke, *Organometallics* **1999**, *18*, 10–20.
[114] W. He, B. O. Patrick, P. Kennepohl, *Nat. Commun.* **2018**, *9*, 3866.
[115] I. Bach, K.-R. Pörschke, R. Goddard, C. Kopiske, C. Krüger, A. Rufińska, K. Seevogel, *Organometallics* **1996**, *15*, 4959–4966.
[116] S. D. Ittel, H. Berke, H. Dietrich, J. Lambrecht, P. Härter, J. Opitz, W. Springer, in *Inorg. Synth. Vol 17* (Ed.: A.G. Macdiarmid), Wiley, **2007**, pp. 117–124.
[117] S. M. Webb, *Phys. Scr.* **2005**, *T115*, 1011–1014.
[118] B. Ravel, M. Newville, *J. Synchrotron Radiat.* **2005**, *12*, 537–541.
[119] M. U. Delgado-Jaime, P. Kennepohl, *J. Synchrotron Radiat.* **2010**, *17*, 119–28.
[120] M. U. Delgado-Jaime, C. P. Mewis, P. Kennepohl, *J. Synchrotron Radiat.* **2010**, *17*, 132–7.